ADVANCED ELECTRONIC MATERIALS
www.advelectronicmat.de



# Ternary Synaptic Plasticity Arising from Memdiode Behavior of $TiO_x$ Single Nanowires

*De Shun Hong, Yuan Sha Chen,* Ji Rong Sun,* and Bao Gen Shen*

**Electric field-induced resistive switching (RS) effect has been widely explored as a novel nonvolatile memory over the past few years. Recently, the RS behavior with continuous transition has received considerable attention for its promising prospect in neuromorphic simulation. Here, the switching characteristics of a planar-structured $TiO_x$ single nanowire device are systematically investigated. It exhibits a strongly history-dependent rectifying behavior that is defined as a "memdiode." It is further demonstrated that a ternary synaptic plasticity could be realized in such $TiO_x$ nanowire device, characterized by the resistance and photocurrent response. For a given state of the memdiode, a conjugated memristive characteristic and a distinct photocurrent can be simultaneously obtained, resulting in a synchronous implementation of various Hebbian plasticities with the same temporal order of spikes. These intriguing properties of $TiO_x$ memdiode provide a feasible way toward the designing of multifunctional electronic synapses as well as programmable artificial neural network.**

## 1. Introduction

Electric field-induced resistance switching (RS) in metal–insulator–metal (MIM) capacitors has attracted tremendous interests due to its potential applications in data storage, reconfigurable logic, particularly artificial neuromorphic computation,[1–4] where the insulative layer can be binary metal oxides, perovskite oxides, and organic polymers.[5–11] As reported, the resistive states of RS device can be tuned by DC sweeping or voltage pulses, undergoing either an abrupt or a continuous transition. The abrupt resistive transition of RS device usually leads to a definite high-to-low resistance ratio, a good endurance, and a long retention. It has been the focus of intensive studies due to the potential application in nonvolatile memory.[5–13] In recent years, continuous resistive transition has attracted increasing attention because of its promising prospect in neuromorphic simulation. For the continuous transition case, the device conductance evolves smoothly with sequential pulsed stimuli or repeated electrical cyclings,[14] resulting in resistive states very sensitive to electrical history and charge flux. This unique characteristic leads to the most important application of this kind of devices, i.e., the implementation of biological synapse for artificial neuromorphic computation. In brain-like neural networks, large amounts of neurons are connected through the synapses. These synapses can transfer information with tunable weight, leading to the capability of learning and memory. Compared with the conventional digital computers based on von Neumann architecture, the brain-inspired neuromorphic computation is much more efficient in processing imprecise or mass data because of its intrinsic superiorities, such as massive-parallelism, error-tolerant, and energy-dissipation.[15] Although the functionality and plasticity of two-terminal synapse have already been imitated in various memristors,[16–26] we noticed that a single device usually exhibited a definite form of Hebbian plasticity. Multidimensional imitations of the synaptic plasticity by analogue memristive devices are less concerned. Obviously, the multidimensional synaptic plasticity has an advantage over the single one for developing electronic synapses with higher integration density but low power consumption, thus it is beneficial to the practical implementation in large-scale neural networks.[27,28]

Synergistically integrating multiple physical effects into an individual electronic device with low dimensionality has been a hot topic over the past few decades.[29,30] Due to confined dimensionality and size effect, nanostructured devices would demonstrate unusual functionalities compared with bulk materials, particularly when they act as detectors or sensors.[31,32] Titania oxide is one of the notable materials exhibiting typical RS and memristive behaviors. In this oxide, oxygen vacancies ($V_O$'s) were considered as the mobile species driven by external electrical field, forming either $V_O$'s-based conductive filaments (CFs) or oxygen-deficient $TiO_x$ phases with composition gradient.[33,34] The $TiO_x$ nanoscopic devices were also known for their potential applications in optoelectronics and photocatalyst.[35,36] Naturally, the compositional gradient in $TiO_x$ will result in nonlinear *I–V* dependence. This, combining with the sensitive optoelectronic response, may provide us an opportunity to realize intriguing functionalities in $TiO_x$-based nanoscopic devices.

In this work, we demonstrated a ternary synaptic plasticity in $TiO_x$ nanowires, characterized by the resistance and

D. S. Hong, Y. S. Chen, J. R. Sun, B. G. Shen
Beijing National Laboratory for Condensed Matter Physics and Institute of Physics
Chinese Academic of Sciences
Beijing 100190, China
E-mail: yschen@aphy.iphy.ac.cn; jrsun@iphy.ac.cn

DOI: 10.1002/aelm.201500359

  

photocurrent of a memdiode that exhibited a strongly history-dependent rectifying behavior. For a given state of the memdiode, conjugated memristive characteristics and a distinct photocurrent can be simultaneously obtained, resulting in a synchronous implementation of various Hebbian plasticities with the same temporal order of spikes. More interestingly, such synaptic plasticity is caused by non-overlapping pulses, which could be understood by the thermal assisted migration of $V_O$'s. This unique property of the $TiO_x$ memdiode provides a feasible way toward the designing of multifunctional electronic synapses as well as programmable artificial neural networks.

## 2. Results and Discussion

In experiments, a planar MIM structure was adopted which facilitated the characterization of microscopic properties for the local switching region. $TiO_2$ nanowires were first synthesized by electrospinning method as described in previous literature.[37] Then, a single nanowire was transferred onto the $SrTiO_3$ substrate that is partially covered by parallel $SrRuO_3$ (SRO) electrodes with 20 μm separations, forming a series of two-terminal nanodevices. These planar devices were sequentially calcined at 500 °C in air to remove organic composite and annealed at 400 °C in vacuum to form oxygen-deficient $TiO_x$ nanowire. **Figure 1**a is a scanning electron microscopy (SEM) image that indicates the rather smooth surface of $TiO_x$ nanowire with a diameter of ≈100 nm. The electric transport behavior was measured by two-terminal method: all voltage biases were applied on the left SRO electrode while the right SRO electrode was grounded. The pristine $TiO_x$ device demonstrated symmetric linear *I–V* characteristic with a very high resistance (>10 GO). After a forming process (the first electric treatment of an initial device) under a voltage of +200 V bias for 400 s, the nanowire device exhibits a forward rectifying behavior as shown in Figure 1b. The positive current turns on at about +70 V and rapidly grows to hundreds of microampere as voltage increases from 70 to 200 V, while the cutoff current keeps below 5 nA in the whole negative direction. Subsequently applying a negative operation bias of –200 V, fascinatingly, the rectifying direction reverses with other features remaining. The retention performance shown in Figure 1c proves the non-volatile nature of the two states that can both be maintained for more than 1000 s. According to its rectifying direction, the diode is characterized as a forward (F-state) or a reverse state (R-state). Further experiments reveal that the rectifying direction of the diode can also be altered by repeated DC sweeps of the route 0 → +200 V → 0 or 0 → –200 V → 0 (Figure S2, Supporting Information). These results show that the switching phenomenon in this two-terminal $TiO_x$ device is caused by the redirection of the *I–V* characteristics, different from the unipolar or bipolar RS behaviors in usual devices. Moreover, unlike the definite resistance state (high or low) in most RS devices, the reversion of rectifying direction will result in a conjugate switching of the diode

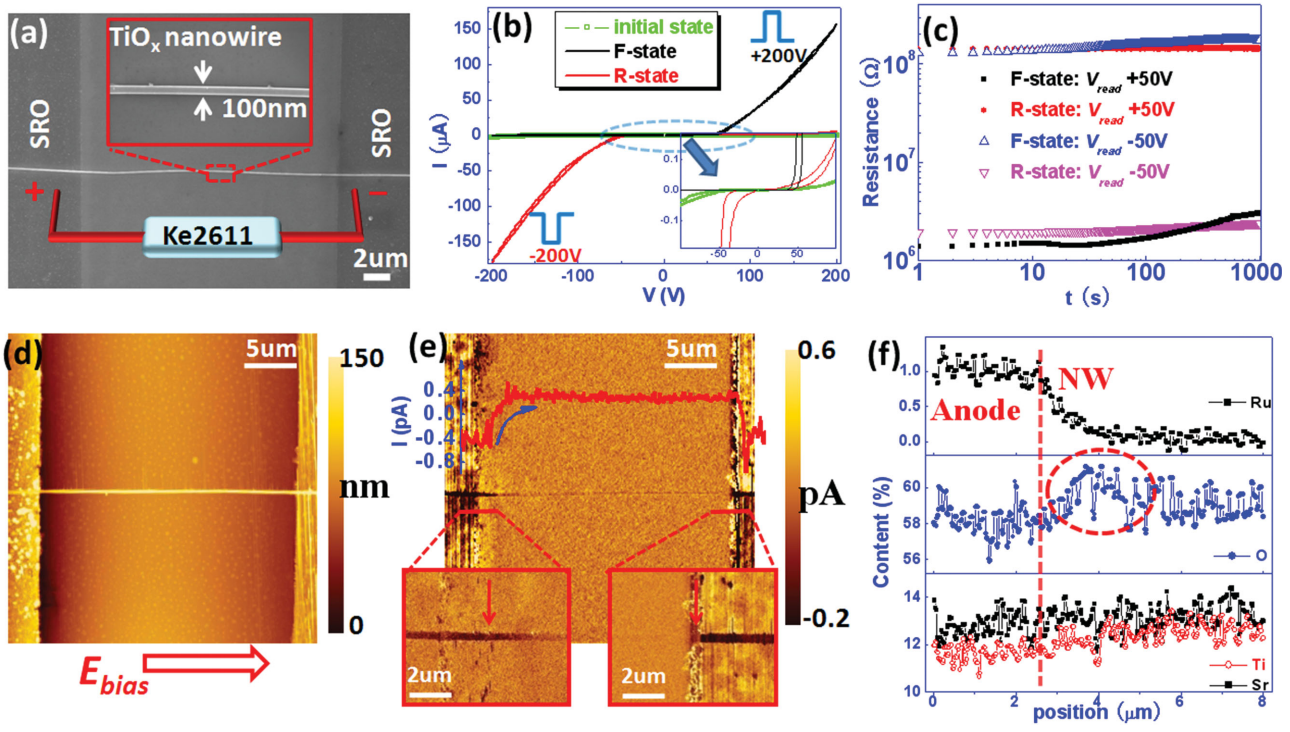


**Figure 1.** a) SEM image of the two-terminal planar device consisted of a $TiO_x$ single nanowire and two SRO electrodes. Inset indicates the diameter of $TiO_x$ nanowire is ≈100 nm. b) Typical *I–V* characteristics of initial state, F-state, and R-state. Inset is magnified image of low voltage region. c) Retention of effective resistance read by ±50 V pulses. Both F-state and R-state possess nonvolatile characteristic. d) Topographic image and e) current mapping image measured by conductive AFM. The top inset in panel (e) shows a line profile of local current along the switched nanowire, while the two bottom insets are magnified mapping images of the anode and cathode regions. The arrows indicate the SRO/$TiO_x$ boundaries. f) EDX line profiles of Ru, O, Ti, and Sr along the nanowire near anode/$TiO_x$ boundary.

resistances read by opposite read voltages. For example, for a flipping from the F- to the R-state, the diode resistance experiences a low-to-high switching for positive read voltage ($V_{read}$) but a high-to-low switching for a negative $V_{read}$.

To clarify the physical origin of rectifying behavior, the microscopic properties of switched $TiO_x$ nanowire were analyzed by the techniques of scanning probe microscopy and energy dispersive X-ray spectroscopy (EDX). Figure 1d presents the surface morphology of device after an electrical forming by +200 V and Figure 1e is the corresponding current mapping measured by a scanning bias of 10 V. The topography of switched nanowire remains uniform, whereas the local current becomes very inhomogeneous, especially near the electrode/$TiO_x$ boundary. In the top inset of Figure 1e, we show the distribution of leakage current along the nanowire. The bottom insets of Figure 1e are magnified mapping results around two electrode/$TiO_x$ interfaces. Apart from the anode, the leakage current exhibits a rapid increase in the first several micrometers and then maintains at a saturation value for further sweeping. This result clearly indicates that there is a relatively insulative region (2–3 μm) formed in the $TiO_x$ nanowire near the anode. To investigate what has happened to this region, the line profiles of the EDX of Ru, O, Ti, and Sr elements were collected. As shown in Figure 1f, the distribution of Sr and Ti is relatively stable in the nanowire, which may indicate the absence of metal ions' migration as reported by Wedig et al. recently.[38] However, an apparent bulge is observed in the line profile of O near the anode/$TiO_x$ boundary, suggesting an accumulation of oxygen ions there. This means that the rectifying behavior of $TiO_x$ device may be caused by the field-induced homogeneous migration of $V_O$'s confined within the nanowire. A possible band diagram of the reversible diode-like behavior is proposed in Figure S3 (Supporting Information). Possibly, vacuum annealing has introduced a number of $V_O$'s into the $TiO_x$ nanowire, and the SRO/$TiO_x$ interfaces of the device could be initially a Schottky-like contact. The concentration of $V_O$'s near the SRO/$TiO_x$ interfaces could be mended by electrical forming and subsequent operations, increasing or decreasing depending on bias polarity. For example, a positive bias on device will drive $V_O$'s to the cathode, leaving nearly stoichiometric $TiO_2$ layer near the anode. As a result, the barrier height will be depressed for the cathode/$TiO_x$ contact and enhanced for the anode/$TiO_x$ contact, leading to the forward rectifying behavior. Contrastingly, an opposite process occurred under negative bias, causing a flipping of rectifying characteristics.

To get further information on $V_O$'s re-distribution and its effect, we studied the correspondence between *I–V* characteristics and photocurrent in the process of field-induced rectification reversion. At first, a positive-negative-positive voltage chain was applied on the device to flip the rectifying direction in sequence, and then the output current and photocurrent were simultaneously measured. We divided the whole process into 14 steps as marked in **Figure 2**a. At each step, we temporarily shut off the bias voltage and quickly measured the *I–V* characteristics of current state. Figure 2b–e shows the *I–V* relations for four typical steps, 1, 6, 10, and 14 (other data are given in Figure S4, Supporting Information), corresponding to R-state, F-state, R-state, and F-state, respectively. Figure 2f shows the short-circuit transient photocurrents ($I_{photo}$) corresponding to the 14 different states, measured when device was illuminated by a laser of 200 mW $cm^{-2}$ (monochromatic light of wavelength 400 nm). It can be seen that the photocurrent is positive in the initial R-state, ≈60 pA, gradually decreased with biased time, and finally turned to a negative value of −50 pA in the F-state. With the reversion of the rectifying direction, the polarity of photocurrent reverses accordingly, indicating a change in built-in electrical field of the $TiO_x$/SRO contact. What should be noted is the different dynamic behavior of the output current and photocurrent in the reversion process. In this process, the output current keeps a continuous increase with biased time, whereas the photocurrent varies rapidly in the beginning of the direction revision but slowly afterward. For instance, from step 1 to 2, the output current increased from 1.4 to 8 nA, about 0.04% of the total change,[39] whereas photocurrent drops from 65 to 3 pA, changing nearly ≈95%. On the contrary, when output current alters rapidly with further biasing, photocurrent varies slightly. Obviously, these two quantities provide two different descriptions for the switching process of the $TiO_x$ device.

The $TiO_x$ nanowire was further programmed by a serial of voltage pulse trains with the amplitude of 200 V and width of 1 s (pulse separation = 50 ms), and the switching resistance was measured after each operation pulse by two additional lower pulses (±50 V with 1 ms width). As shown in **Figure 3**a, the diode resistances read by positive ($R_+$) and negative ($R_-$) $V_{read}$ exhibit a bidirectional evolution driven by the consecutive switching pulses. Under the impact of 250 negative pulses and 250 positive pulses, $R_+$ gradually increases from 2 MΩ to 80 GΩ and decreases to 2 MΩ again. Correspondingly, $R_-$ changes from 200 GΩ to 2 MΩ and back to 200 GΩ. This process well repeats when repeating the pulse trains (Figure 3b), demonstrating good reproducibility of the RS behavior. To get a quantitative description of the flipping process of rectification, the $R_+/R_-$ ratio as a function of switching cycles is presented in Figure 3c, triggered by the alternative pulse trains. It is $10^{-5}$ in the starting state, and rapidly increases upon the impact of negative pulses, indicating a weakening of the rectifying characteristic of the device. After reaching the state of $R_+/R_- = 1$, where the device becomes symmetric to opposite biases, the $R_+/R_-$ ratio, through a slight inflection point, goes rapidly into the range well above 1, signaling the reversion of rectifying direction. Obviously, the device can be driven to any intermediate state between the F- and the R-states by an appropriate pulse train and stays there without further programming, and may be called as "memdiode." Corresponding to the variation of $R_+/R_-$ ratio, photocurrent also exhibits an oscillation as shown in Figure 3d. Although it demonstrates a relatively larger fluctuation than $R_-$ or $R_+$, the reversed rectification of the device can still be clearly identified. Comparing with common electrical reading method, the photocurrent reading is non-perturbative and consumes lower power (≈4 nW) that are both beneficial for the device design. In addition, photoelectrical reading gives a characterization of the zero-bias state for the memdiode device, which is different from either positive or negative electric voltages.

As well established, the memristor is a promising candidate for electronic synapse, acting as an important hinge element in artificial neural network. Its gradually evolved resistance can be regarded a response to external stress of the synaptic

  

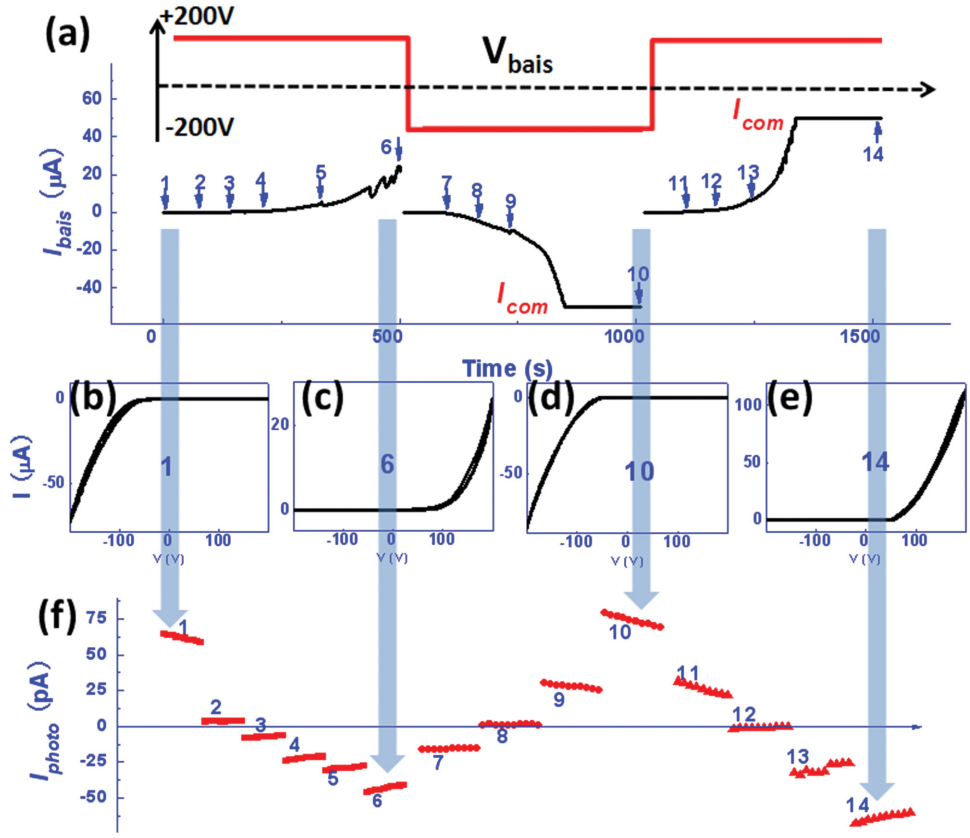


**Figure 2.** a) Operation bias sequence of +200 V → –200 V → +200 V and the output current (current compliance is 50 μA). Numbers indicate the multiple switching steps. b–e) *IV* curves measured at the turning points, indicating the initial R-state (step 1) is flipped to F-state (step 6), to R-state (step 10) and to F-state (step 14). f) Photocurrent corresponding to 1–14 switching steps measured under the illumination of 400 nm laser. Positive $I_{photo}$ is obtained in R-state while negative $I_{photo}$ for F-state.

connection, emulating the adjustable weight of biological synapses. Hereafter, we will demonstrate that, basing on its memdiode behavior and the different state reading approaches, the $TiO_x$ nanowires can lead to ternary imitations of the synaptic plasticity. Figure 3e is the forming processes of three devices under different pulse voltages (80, 100, and 120 V). These behaviors are analogous to the training effect of memristors. Both speed and magnitude of the resistive switching increase with pulse amplitude, well mimicking the faster responses of synapse to enhanced neurostimulant. Moreover, we find that the initial $V_O$'s concentration of $TiO_x$ nanowire has a huge influence on the training process (Figure S5, Supporting Information), which implies a feasible way for reducing the programming voltage in the practical application.

The most important capabilities of the biological synapses are perception and learning. The well-known learning rule is called "spike timing dependence plasticity" (STDP), meaning that the strength of synaptic connection can be regulated by the relative spike timing between pre- and post-neurostimulants. As illustrated in **Figure 4**a, the memdiode can act as a synapse while the two electrodes act as pre- and post-neurons that import nerve impulses. In our electric measurements, the voltage pulses were always applied on the left side electrode (pre-neuron). Thus, to simulate the spike timing process of the pre-/post-impulses, the positive-negative pulse trains with various intervals ($\Delta t$) were applied on the pre-neuron while the post-neuron was grounded. Unlike the overlapping pulse spikes used in most of previous works, the pre- and post-spikes in our experiments are kept strictly separate from each other, which is more closer to the biological reality. The synaptic weights were quantified, respectively, by the resistance and photocurrent of the memdiode. Three quantities, $\Delta R_-/R_-$, $\Delta R_+/R_+$, and $\Delta I/I$ are simultaneously determined for each impulse separation. Here, the relative change of synaptic weights are defined as $\frac{\Delta R}{R}=\frac{R_{\Delta t}-R_{\Delta t\to\infty}}{R_{\Delta t\to\infty}}$ and $\frac{\Delta I}{I}=\frac{I_{\Delta t}-I_{\Delta t\to\infty}}{I_{\Delta t\to\infty}}$, respectively. Figure 4b shows $\Delta R_-/R_-$ as a function of spike separation, and the standard STDP characteristic was observed: The rapid decrease of $\Delta R_-/R$ as $\Delta t$ approaches zero along positive axis indicates a strengthening of the synapse connection when the pre-spike is slightly preceded to the post-one. This phenomenon is usually referred as long-term potentiation (LTP). In contrast, $\Delta R_-/R_-$ increases when $\Delta t$ approaches zero along negative axis, signaling a weakening of the synaptic connection when post-spike appears before the pre-one. This phenomenon is called as long-term depression (LTD). Fascinatingly, the simultaneously recorded $\Delta R_+/R_+ - \Delta t$ relation displays an anti-STDP dependence, i.e., opposite dependency of LTP and LTD can be achieved either by changing the order of stimuli or the polarity of the

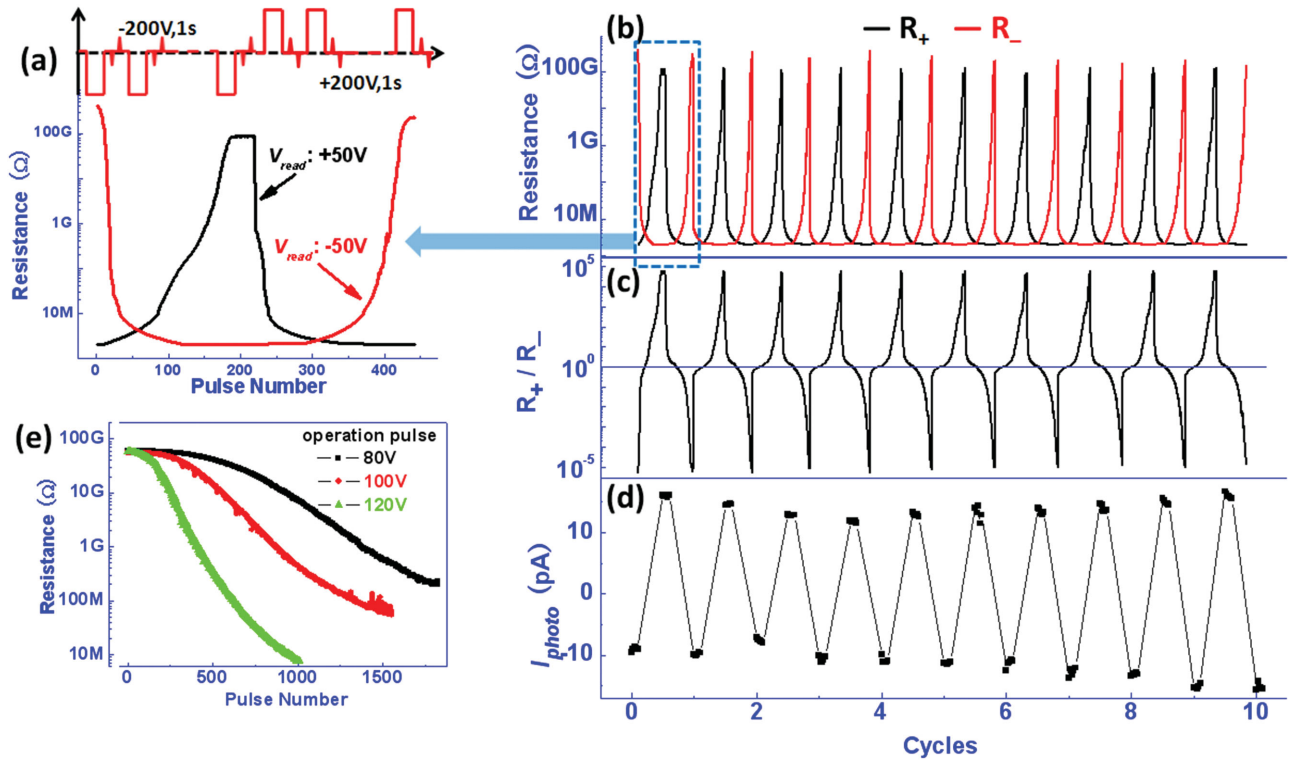


**Figure 3.** a) Device resistance demonstrates continuous change with the number of operation pulses. And the $R_+$ and $R_-$ measured by ±50 V read pulses possess the conjugated memristive behaviors. Endurance performance of b) $R_+$ and $R_-$, c) $R_+/R_-$ ratio, and d) photocurrent response during ten switching cycles. e) Three forming processes triggered by 80, 100, and 120 V pulse amplitudes, emulating the training effect of synaptic device.

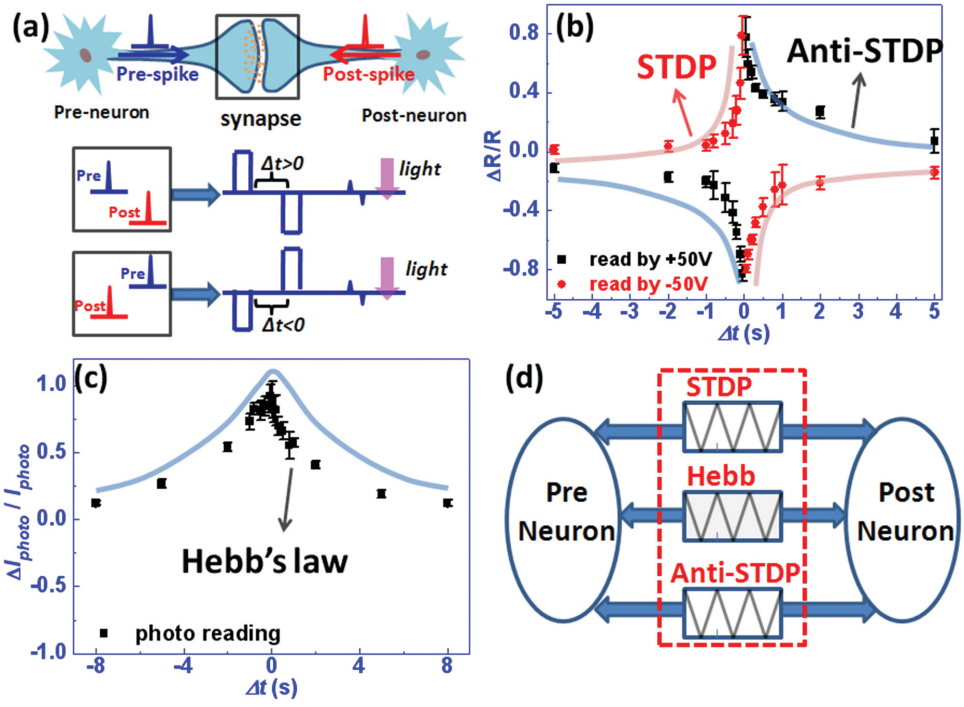


**Figure 4.** a) Schematic illustration of synaptic plasticity between a pre-neuron and a post-neuron, and the waveforms for implementing the spike timing rules in our experiments. b) The STDP, anti-STDP and (c) Hebbian forms were synchronously achieved in one $TiO_x$ nanowire device when the synaptic weights were determined by positive read pulse, negative read pulse, and photocurrent. d) Schematic view of the ternary synaptic plasticity of $TiO_x$ memdiode device.

read pulses. Moreover, if the synaptic weight is determined by photocurrent, a symmetric distribution of $\Delta I_{photo}/I_{photo}$ is obtained for the positive and negative $\Delta t$ (Figure 4c), which indicates that the synaptic strength is affected by the impulse separation rather than impulse order. This is the well-known Hebb's law, also a basic form of the synaptic plasticity. The above results show that, basing on a single synaptic device that has the memdiode characteristic, the ternary synaptic plasticity can be realized. Figure 4d is schematic showing of the ternary synaptic plasticity. Considering the fact that the STDP scheme is basic for determining the functionality and/or type of synapses, the diverse STDP forms implemented in a single device will expand the function and computation logic of electronic synapse, implying the prospect of programmable artificial neural networks.

Such spike time dependence caused by non-overlapping pulses can be understood by the thermal assisted migration of $V_O$'s that was reported in our earlier work.[40] In the bipolar switching, we demonstrated that the Joule heating effect of last reset pulse could influence the following set operation, where a shorter interval between reset-set pulses would lead to a fast switching speed or a lower set voltage. In the STDP measurement, $\Delta t$ approaching zero will reduce the thermal dissipation that accumulated in first operation pulse, and raise the effective temperature of second pulse. Thus, the $V_O$'s migration during second pulse is strengthened accordingly due to the higher ion mobility. For example, when $\Delta t$ approaches zero along positive axis, the trend of R-state of the memdiode is enhanced by the second negative pulse, resulting in higher $R_+$ and lower $R_-$. And obviously, reversed variations of $R_+$ and $R_-$ will be observed when $\Delta t < 0$. Similar result was also reported by Kim et al. in the resistive $Ta_2O_{5-x}$ film and it was called as second-order memristor effect.[41]

## 3. Conclusion

In summary, we demonstrated a ternary synaptic plasticity in $TiO_x$ nanowires, characterized by the resistance and photocurrent of a memdiode. We showed that the oxygen vacancies in the nanowire underwent a re-distribution under the driving of electric field, yielding a diode behavior. We called the diode as memdiode since it could be modulated to any intermediate state between a forward and a reverse rectification states, and stayed there without further programming. The forward and reverse diode resistances and the photocurrent of the memdiode yielded different characterizations to external electrical stimuli. Based on this, the multidimensional synaptic plasticity of the forms of STDP, anti-STDP, and Hebb's law was implemented in a single memdiode device. These intriguing properties of the $TiO_x$ nanowire pave a new way toward the designing of high density and low power consumption electronic synapses as well as the programmable artificial neural networks.

## 4. Experimental Section

*Sample Preparation*: A 50 nm $SrRuO_3$ (SRO) film was deposited on the $SrTiO_3$ (STO) substrate at 680 °C by pulsed laser deposition technique and patterned to parallel strip electrodes with 20 μm separations by conventional photolithography process. $TiO_2$ nanowires were synthesized by electrospinning method as described in previous literature.[37] The $TiO_2$/poly(vinyl pyrrolidone) (PVP) composite nanofibers were first electrospun from the mixed sol-gel precursor containing titanium tetraisopropoxide ($Ti(OiPr)_4$), PVP polymer, acetic acid, and ethanol. To form two-terminal planar devices, a single nanowire was picked and transferred onto STO substrate that perpendicularly crossed the SRO strips. Then, the $TiO_2$/PVP composite based nanowire device was calcined in air at 500 °C for 3 h to remove the PVP and form anatase $TiO_2$ phase. Finally, to introduce oxygen vacancies into the single nanowire and form oxygen-deficient $TiO_x$ phases, the whole device was further annealed in vacuum at 400 °C for 15 min.

*Characterization*: The electric characteristics were measured by Keithley 2611 SourceMeter and Agilent 81150A Pulse Generator at room temperature. All voltage biases were applied on the left SRO electrode while the right SRO electrode was grounded. The photoelectric response of nanowire device was illuminated by monochromatic light of wavelength 400 nm and intensity 200 mW $cm^{-2}$ from a laser diode driver. The crystal structure of calcined nanofibers was confirmed by X-ray diffraction (Bruker D2 Phaser) and the average diameter was measured by an SEM (Hitachi S-4800). The XRD and SEM results (Figure S1, Supporting Information) indicate that the as-prepared $TiO_x$ nanowires were consisted of pure anatase phase with diameters ranging from 50 to 200 nm. Surface morphology and conductance of the planar device were analyzed by a scanning probe microscopy (Seiko SPA400). In current mapping experiment, the scanning bias was applied on the two electrodes synchronously and the Au probe was grounded. The elemental spatial profile of switched nanowire was recorded by an energy dispersive X-ray spectrometer equipped in the SEM.

## Supporting Information

Supporting Information is available from the Wiley Online Library or from the author.

## Acknowledgements

This work was partially supported by the National Basic Research of China (2013CB921700), the "Strategic Priority Research Program (B)" of the Chinese Academy of Sciences (XDB07030200), and the National Natural Science Foundation of China (11374339).

Received: October 20, 2015
Revised: December 9, 2015
Published online: January 13, 2016

[1] R. Waser, M. Aono, *Nat. Mater.* **2007**, *6*, 833.
[2] J. Borghetti, G. S. Snider, P. J. Kuekes, J. J. Yang, D. R. Stewart, R. S. Williams, *Nature* **2010**, *464*, 873.
[3] S. D. Ha, D. B. Strukov, *J. Appl. Phys.* **2011**, *110*, 071101.
[4] J. J. Yang, D. B. Strukov, D. R. Stewart, *Nat. Nanotechnol.* **2012**, *8*, 13.
[5] S. Q. Liu, N. J. Wu, A. Ignatiev, *Appl. Phys. Lett.* **2000**, *76*, 2749.
[6] S. Seo, M. J. Lee, D. H. Seo, E. J. Jeoung, D.-S. Suh, Y. S. Joung, I. K. Yoo, I. R. Hwang, S. H. Kim, I. S. Byun, J.-S. Kim, J. S. Choi, B. H. Park, *Appl. Phys. Lett.* **2004**, *85*, 5655.
[7] I. Baek, M. Lee, S. Seo, M. Lee, D. Seo, D. S. Suh, J. Park, S. Park, H. Kim, I. Yoo, U. I. Chung, J. Moon, *Tech. Dig. Int. Electron Devices Meet.* **2004**, 587.
[8] B. J. Choi, D. S. Jeong, S. K. Kim, C. Rohde, S. Choi, J. H. Oh, H. J. Kim, C. S. Hwang, K. Szot, R. Waser, B. Reichenberg, S. Tiedke, *J. Appl. Phys.* **2005**, *98*, 033715.

[9] K. Szot, W. Speier, G. Bihlmayer, R. Waser, *Nat. Mater.* **2006**, *5*, 312.
[10] S. B. Lee, S. C. Chae, S. H. Chang, J. S. Lee, S. Seo, B. Kahng, T. W. Noh, *Appl. Phys. Lett.* **2008**, *93*, 212105.
[11] B. Cho, T. W. Kim, S. Song, Y. Ji, M. Jo, H. Hwang, G. Y. Jung, T. Lee, *Adv. Mater.* **2010**, *22*, 1228.
[12] Y. C. Yang, F. Pan, Q. Liu, M. Liu, F. Zeng, *Nano Lett.* **2009**, *9*, 1636.
[13] R. Waser, R. Dittmann, G. Staikov, K. Szot, *Adv. Mater.* **2009**, *21*, 2632.
[14] D. B. Strukov, G. S. Snider, D. R. Stewart, R. S. Williams, *Nature* **2008**, *453*, 80.
[15] C. Mead, *Proc. IEEE* **1990**, *78*, 1629.
[16] K. Seo, I. Kim, S. Jung, M. Jo, S. Park, J. Park, J. Shin, K. P. Biju, J. Kong, K. Lee, B. Lee, H. Hwang, *Nanotechnology* **2011**, *22*, 254023.
[17] P. Krzystecko, J. Münchenberger, M. Schäfers, G. Reiss, A. Thomas, *Adv. Mater.* **2012**, *24*, 762.
[18] A. Nayak, T. Ohno, T. Tsuruoka, K. Terabe, T. Hasegawa, J. K. Gimzewski, M. Aono, *Adv. Funct. Mater.* **2012**, *22*, 3606.
[19] T. Tsuruoka, T. Hasegawa, K. Terabe, M. Aono, *Nanotechnology* **2012**, *23*, 435705.
[20] S. Part, J. Noh, M. Choo, A. M. Sheri, M. Chang, Y. B. Kim, C. J. Kim, M. Jeon, B. G. Lee, B. H. Lee, H. Hwang, *Nanotechnology* **2013**, *24*, 384009.
[21] S. Part, J. Noh, M. Choo, A. M. Sheri, M. Chang, Y. B. Kim, C. J. Kim, M. Jeon, B. G. Lee, B. H. Lee, H. Hwang, *Nanotechnology* **2013**, *24*, 384009.
[22] S. Li, F. Zeng, C. Chen, H. Liu, G. Tang, S. Gao, C. Song, Y. Lin, F. Pan, D. Guo, *J. Mater. Chem. C* **2013**, *1*, 5292.
[23] F. Alibart, E. Zamanidoost, D. B. Strukov, *Nat. Commun.* **2013**, *4*, 2072.
[24] S. Ambrogio, S. Balatti, F. Nardi, S. Facchinetti, D. Ielmini, *Nanotechnology* **2013**, *24*, 384012.
[25] D. S. Jeong, I. Kim, M. Ziegler, H. Kohlstedt, *RSC Adv.* **2013**, *3*, 3169.
[26] S. Kim, S. H. Choi, W. Lu, *ACS Nano* **2014**, *8*, 2369.
[27] S. M. Yu, B. Gao, Z. Fang, H. Y. Yu, J. F. Kang, H.-S. P. Wong, *Adv. Mater.* **2013**, *25*, 1774.
[28] B. Gao, Y. J. Bi, H. Y. Chen, R. Liu, P. Huang, B. Chen, L. F. Liu, X. Y. Liu, S. M. Yu, H. -S. P. Wong, J. F. Kang, *ACS Nano* **2014**, *8*, 6998.
[29] Y. N. Xia, P. D. Yang, Y. G. Sun, Y. Y. Wu, B. Gates, Y. D. Yin, F. Kim, H. Q. Yan, *Adv. Mater.* **2003**, *15*, 353.
[30] C. M. Liber, Z. L. Wang, *MRS Bull.* **2007**, *32*, 99.
[31] A. Kolmakov, M. Moskovits, *Annu. Rev. Mater. Res.* **2004**, *34*, 151.
[32] T. Y. Zhai, X. S. Fang, M. Y. Liao, X. J. Xu, H. B. Zeng, Y. Bando, D. A. Golberg, *Sensors* **2009**, *9*, 6504.
[33] J. J. Yang, M. D. Pickett, X. Li, D. A. A. Ohlberg, D. R. Stewart, R. S. Williams, *Nat. Nanotechnol.* **2008**, *3*, 429.
[34] D.-H. Kwon, K. M. Kim, J. H. Jang, J. M. Jeon, M. H. Lee, G. H. Kim, X.-S. Li, G.-S. Park, B. Lee, S. Han, M. Kim, C. S. Hwang, *Nat. Nanotechnol.* **2010**, *5*, 148.
[35] A. L. Linsebigler, G. Q. Lu, J. T. Yates, *Appl. Chem. Rev.* **1995**, *95*, 735.
[36] Y. G. Han, G. Wu, M. Wang, H. Z. Chen, *Appl. Surf. Sci.* **2009**, *256*, 1530.
[37] D. Li, Y. N. Xia, *Nano Lett.* **2003**, *3*, 555.
[38] A. Wedig, M. Luebben, D. Y. Cho, M. Moors, K Skaja, V. Rana, T. Hasegawa, K. K. Adepalli, B. Yildiz, R. Waser, I. Valov, *Nat. Nanotechnol.* **2015**, *221*, 1.
[39] The total change of output current, from 1.4 nA of step 1 to 21 μA of step 6, is about 15 000 times.
[40] M. G. Cao, Y. S. Chen, J. R. Sun, D. S. Shang, L. F. Liu, J. F. Kang, B. G. Shen, *Appl. Phys. Lett.* **2012**, *101*, 203502.
[41] S. Kim, C. Du, P. k. Sheridan, W. Ma, S. Choi, W. D. Lu, *Nano Lett.* **2015**, *15*, 2203.

  